



## The COAST $\ell$ OOO project dataset

Philippe Massicotte<sup>1</sup>, Marcel Babin<sup>4, 1</sup>, Frank Fell<sup>2</sup>, Vincent Fournier-Sicre<sup>3, 5</sup>, and David Doxaran<sup>4</sup>

<sup>1</sup>\*Takuvik International Research Laboratory (IRL 3376) ULaval - CNRS, Biology department, Laval University, Quebec, Canada

<sup>2</sup>Informus GmbH, Berlin, Germany

<sup>3</sup>ACRI-ST 260 Route du Pin Montard, 06904 Sophia-Antipolis, France Phone: +33 4 92 96 75 00

<sup>4</sup>Laboratoire d'Océanographie de Villefranche, CNRS / Sorbonne Université, Villefranche-sur-mer, France

<sup>5</sup>\*Data Processing Systems Procurement Manager European Organisation for the Exploitation of Meteorological Satellites (EUMETSAT) EUMETSAT-Allee 1, 64295 Darmstadt, Germany Office: +49 6151 807 7336 Mobile: +49 151 174 38520

**Correspondence:** Marcel Babin (marcel.babin@takuvik.ulaval.ca)

**Abstract.** Coastal Surveillance Through Observation of Ocean Color (COAST $\ell$ OOO) oceanographic expeditions were conducted in 1997 and 1998 to examine the relationship between the optical properties of seawater and related biological and chemical properties across the coastal-to-open ocean gradient along the European coasts. A total of 379 stations were visited along the coasts of the Gulf of Lion in the Mediterranean Sea ( $n = 61$ ), Adriatic Sea ( $n = 39$ ), Baltic Sea ( $n = 57$ ), North Sea  
5 ( $n = 99$ ), English Channel ( $n = 85$ ) and Atlantic Ocean ( $n = 38$ ). A particular emphasis has been dedicated to the collection of a comprehensive set of apparent (AOPs) and inherent (IOPs) optical properties to support the development of ocean color remote sensing algorithms. The data were collected in situ using traditional ship-based sampling, but also from a helicopter, which is a very efficient means for that type of coastal sampling. The dataset collected during the COAST $\ell$ OOO campaigns is still today quite unique in that it is fully consistent in terms of operators, protocols, and instrumentation. This rich and historical  
10 dataset is still today frequently requested and used by other researchers. Therefore, we present the result of an effort to compile and standardize a dataset which will facilitate their reuse in future development and evaluation of new bio-optical models adapted for optically-complex waters. The dataset is available at <https://doi.org/10.17882/93570> (Massicotte et al., 2023).

### 1 Introduction

Since the launch of the Coastal Zone Color Scanner (CZCS) by NASA in 1978, ocean color remote sensing has been used to  
15 monitor the state of, and the changes in global marine ecosystems both in time and space. In open oceans, the main component that affects the variations in the inherent (IOPs) and apparent (AOPs) optical properties of seawater is phytoplankton, which is usually represented by the concentration of chlorophyll *a* (Morel and Prieur, 1977). Such open ocean waters are traditionally termed Case 1 waters. Many simple empirical spectral band ratio algorithms have been developed to link changes in remotely-sensed ocean color (OC), measured as reflectance, to the variations in chlorophyll *a* concentration (see O'Reilly and Werdell  
20 2019 for an extensive evaluation of OC band ratio algorithms). Because these algorithms perform surprisingly well, a plethora

---

\*Current address

\*Current address



of studies have been conducted based on it, notably about phytoplankton phenology (e.g., Vargas et al. 2009) and phytoplankton primary production (see Carr et al. 2006 and references therein).

Space-borne monitoring of aquatic ecosystems is more challenging for optically complex Case 2 waters (Morel and Prieur, 1977) often found in coastal areas. In contrast to Case 1 waters, the optical properties of Case 2 waters are determined by several types of constituents occurring in highly variable concentrations. Inland rivers typically drain large catchment areas that deliver important quantities of optically significant substances such as chromophoric dissolved organic matter (CDOM) and suspended particulate matter (SPM) to the coastal waters (Hedges et al., 1997; Cole et al., 2007; Massicotte et al., 2017). In these areas, bottom reflectance and resuspension of sediments can also alter the signal of water-leaving reflectance (Lee et al., 1998). Because CDOM and SPM do not necessarily covary with chlorophyll *a* and can mask the signal from phytoplankton (Sat, 2000), bio-optical algorithms developed for Case 1 waters are generally not appropriate for optically-complex Case 2 waters (Gordon and Morel, 1983). Hence, in situ measurements of optically active components (CDOM, SPM, chlorophyll *a*), related radiometric quantities, AOPs and IOPs are, even to this day, critically needed to develop and improve bio-optical algorithms for coastal areas.

The objective of the Coastal Surveillance Through Observation of Ocean Color (COAST $\ell$ OOC) oceanographic expeditions was to acquire a comprehensive set of AOPs and IOPs along the European coasts. Concentrations of the optically significant components were also collected to help the development of new remote sensing algorithms in optically complex waters. Back in 1997 and 1998, the COAST $\ell$ OOC campaigns were among the very first concerted efforts to fill the knowledge gaps in coastal marine optics by establishing a large, homogeneous, and complete optical dataset for coastal waters. A total of 379 stations were visited along the coasts of the Mediterranean, Adriatic, Baltic and North Sea, in the English Channel, and in the Atlantic Ocean, mostly in coastal, but also in open oceanic waters. While this unique set of data has been used or referenced over the years in numerous peer-reviewed publications (see list in Appendix A), a reference final dataset, with well-documented quality controls, has never been published. Even though the COAST $\ell$ OOC campaigns were carried out more than 20 years ago, the rich and historical dataset that has been collected still has great potential to contribute to the development and evaluation of new bio-optical models adapted for optically-complex waters. The goal of this paper is to formally present a quality-controlled and final reference version of the COAST $\ell$ OOC dataset, archived in a public repository where users can download it readily.

## 2 Study area and sampling overview

### 2.1 Study area and general sampling strategy

During the six COAST $\ell$ OOC campaigns, further referred to as C1 to C6, a total of 379 locations were visited (Fig. 1). The stations were located along the coasts of the Gulf of Lion in the Mediterranean Sea ( $n = 61$ ), Adriatic Sea ( $n = 39$ ), Baltic Sea ( $n = 57$ ), North Sea ( $n = 99$ ), English Channel ( $n = 85$ ) and Atlantic Ocean ( $n = 38$ ). Within each area, the stations were generally distributed along across-shore or along-shore transects to capture the land-to-sea gradients and document river plumes (Fig. 1B). COAST $\ell$ OOC campaigns were either ship-based (C1, C4, C5) or used a helicopter as a sampling platform (C2, C3, C6) between 1997-04-02 and 1998-09-25 (Fig. 2A). Compared to traditional ship-based sampling, the helicopter



platform allowed to efficiently sample stations close to the coast in areas difficult to access by boat (some samples were collected in waters as shallow as 1 m, Babin 2003). Combining both ship and airborne sampling approaches allowed covering the whole inshore to open-ocean aquatic continuum. The bathymetry (GEBCO Bathymetric Compilation Group 2020, 2020) varied greatly across the stations, where it averaged 10 meters in the Adriatic Sea and 2600 meters in the Case 1 Mediterranean Sea (Fig. 2B).

## 2.2 Data collection

At each site, between six and eight liters of water just below the surface were collected using either Niskin or polyethylene bottles for laboratory analyses. Water samples collected onboard the ship were immediately processed, or within two hours if sampled using the helicopter (see Babin 2003 for further details).

## 2.3 Suspended particulate matter and pigments

On board the ship, water samples were analyzed and/or stored immediately after collection. When using a helicopter as a sampling platform, water samples were kept in six liters polyethylene containers no longer than two hours after sampling. Filtration was conducted at low vacuum onto 25 mm glass fiber filters (Whatman, GF/F) to collect particles for subsequent analyses, as described below. Three separate subsamples (up to two liters each) were filtered for each sample with the following purposes. To determine the concentration of suspended particulate matter (SPM;  $\text{g m}^{-3}$ ), the particles collected onto a pre-weighed GF/F filter were dried and stored in a freezer at  $-80\text{ }^{\circ}\text{C}$  until the dry weight was determined less than two months later in the laboratory (Van Der Linde, 1998). For pigment analysis, the filter with collected particles was inserted into a cryotube and kept in liquid nitrogen until analysis less than three months later. High-performance liquid chromatography (HPLC) was used as described by Vidussi et al. 1996 to determine liposoluble pigment concentrations. Total chlorophyll *a* is here defined as the sum of chlorophyll *a*, divinyl-chlorophyll *a*, chlorophyll *a* isomer and epimer, chlorophyllids *a*, and phaeopigments. The concentrations of particulate organic carbon and nitrogen (POC and PON, respectively) were determined using a Carlo Erba NCS 2500 elemental analyzer as described in Ferrari et al. 2003. These determinations were made on particles collected onto a GF/F filter precombusted at  $450\text{ }^{\circ}\text{C}$  for 2 h and stored in the freezer at  $-80\text{ }^{\circ}\text{C}$  until analysis less than two months later. Further details concerning laboratory analyses can be found in Babin 2003; Ferrari 2000; Ferrari et al. 2003. To determine the concentration of dissolved organic matter (DOC, M), seawater samples were filtered on a 0.22 mm Millipore membrane. The final filtrate was transferred to a 100-mL amber-glass bottle, stored in the refrigerator and analyzed within 3 weeks. DOC was determined by high temperature catalytic oxidation using a Carlo Erba 480 analyzer. The methodological details can be found in Ferrari 2000.

## 2.4 Optical measurements

At each station, an optical package was deployed in the water column from the surface, down to a few meters above the ocean bottom in shallow waters, and to maximum depths of ca. 100 m in deep waters. The deployed package included a CTD



85 (conductivity, temperature, and depth) as well as an array of optical instruments to simultaneously measure the coefficients of beam attenuation, absorption and scattering, and irradiance in the water column. The Modular Data and Power System (MODAPS) data-gathering system from Wetlabs Inc., USA was used to combine the time-stamped data from the different instruments to produce a data matrix with a common depth grid. For further information, please refer to the COAST $\ell$ OOC final report (Aiken et al., 2022).

90 A specific aspect of COAST $\ell$ OOC is the use of a helicopter as a sampling platform, which has enabled high-frequency visiting of sites in very shallow waters (see section 2.1). A drawback of this approach is the difficulty to operate a helicopter stationary at a constant height, especially at low or varying wind speeds. This can result in vertical movements of the instrument package in water on the order of 1-2 m s<sup>-1</sup>. To ensure the availability of data of sufficient quality close to the surface, several consecutive up- and downcasts were performed at each “helicopter” site. Across all the measured vertical profiles, the most  
95 suitable casts for depth merging and surface extrapolation (not necessarily the same) were selected.

#### 2.4.1 Irradiance measurements

The SeaWiFS Profiling Multichannel Radiometer (SPMR, Satlantic Inc, Canada) was used to measure the downward ( $E_d$ , W m<sup>-2</sup>  $\mu$ m<sup>-1</sup>) and upward ( $E_u$ , W m<sup>-2</sup>  $\mu$ m<sup>-1</sup>) irradiances in the water column.  $E_d$  and  $E_u$  at a total of 13 wavelengths from the blue part of the spectrum (ca. 410 nm) to the near-infrared (ca. 865 nm) were measured at a rate of 6 Hz. The actual  
100 wavelengths differ slightly between upward and downward observations. Also, the set of nominal wavelengths were partly modified after campaign no. 1 (i.e., for campaigns 2 to 6) to better match the MERIS satellite channels (see below). For the ship-based measurements, concomitant observations of the in-air downward spectral irradiance at the sea surface were performed to account for changes in the incoming solar radiation during the in situ profiling (e.g., due to clouds). This approach was not achievable for the helicopter-based measurements, since there was no suitable place to mount the radiometer. For these  
105 campaigns, measurements of  $E_d$  taken by the profiler while in air (before and after the in-water measurements) were used to assess  $E_d$  on the sea surface. In order to minimize the time lag between the in-water measurements and the  $E_d$  values on the sea surface, our processing code automatically chose the air measurements closest in time.

#### 2.4.2 Irradiance surface extrapolation

To calculate the water-leaving reflectance, accurate measurements of both  $E_d$  and  $E_u$  just below the water surface ( $z = 0^-$ ) are  
110 needed. In case no spectrally matching in-air  $E_d$  reference data are available (as is the case for the helicopter-based campaigns), this was done by extrapolating both  $E_d(z)$  and  $E_u(z)$  vertical profiles toward the sea surface by fitting an exponential model for the depth dependence of the measured spectral irradiance values (equation 1):

$$\Gamma(\lambda, z) = \Gamma(\lambda, 0^-) e^{-K_\Gamma(\lambda)z} \quad (1)$$



where  $\Gamma(\lambda, z)$  is either  $E_d$  or  $E_u$  measured at wavelength  $\lambda$  and at depth  $z$ ,  $\Gamma(\lambda, 0^-)$  is  $E_d$  or  $E_u$  estimated at the air-  
115 water interface, and  $K_\Gamma$  is either the estimated diffuse attenuation coefficient for downward ( $K_{Ed}$ ,  $\text{m}^{-1}$ ) or upward ( $K_{Eu}$ ,  $\text{m}^{-1}$ ) irradiance.

In case spectrally matching in-air  $E_d(0^+)$  reference data are available (as is the case for most ship-based campaigns),  $E_d(0^-)$  is calculated from  $E_d(0^+)$  by applying channel-specific air-sea transmission factors. The such derived  $E_u(0^-)$  and  $E_d(0^-)$  values are then used to calculate the water reflectance  $R(0^+)$  just below the sea surface:

$$120 \quad R(0^-) = \frac{E_u(0^-)}{E_d(0^-)} \quad (2)$$

Vertical irradiance profiles in the red and near-infrared channels above 600 nm were fitted using a sum of two exponential functions to account for Raman scattering significantly contributing especially to the upward light field at these wavelengths (e.g., Sugihara et al. 1984). Not doing so will lead to a substantial underestimation of the extrapolated subsurface values due to significant Raman contribution from excitation wavelengths with significantly lower  $K$  values (see Appendix 1).

### 125 2.4.3 Irradiance depth merging

Depth-merged profiles were derived for all sites by applying a standardized approach. The underlying strategy for depth merging was to provide users with the information they need to do their own analyses, while modifying the original data as little as possible. Processing was therefore limited to procedures that could be applied equally to all COAST $\ell$  OOC campaigns, whether helicopter- or ship-based. For example, variations of the incoming solar radiation were not considered in the depth merging  
130 process, since such observations were not available for the helicopter-based campaigns. However, if measured while operating from research vessels, such information is included in the depth-merged profile data to allow users to do their own subsequent analyses.

Typically, several up- and downcast vertical profiles were performed, especially when using the helicopter as a sampling platform, to increase the potential availability of high-quality observations. The actual merging process was executed as follows.  
135 First, any observation not meeting both of the two following conditions was discarded: (1) SPMR instrument tilt smaller than  $20^\circ$  and (2) SPMR vertical speed between 0.1 and  $2.0 \text{ m s}^{-1}$ . To automatically identify the best-suited cast for profile generation, the observations meeting the above two conditions were then distributed cast-wise over 0.2 m wide vertical bins, starting at zero depth. Finally, the cast with the highest number of bins containing at least one valid observation was selected for depth profile generation, if it fulfilled two further conditions: (3) at least 2 m vertical distance between the highest and the lowest bin  
140 and (4) at least 50% of the bins contain at least one observation. No depth merged data is provided for stations where there is no cast meeting all of the above four conditions. Combining several casts of a station has not proven successful due to potentially large discontinuities at depth levels where the number of available casts changes, especially in case of unstable atmospheric conditions with the corresponding short-term irradiance fluctuations.

Actual depth merging was done by taking the median of all observations of a particular irradiance parameter within each  
145 depth bin. Spectral irradiance observations were only considered for values above  $0.01 \text{ W m}^{-2} \mu\text{m}^{-1}$  to reduce the impacts of



potentially inaccurate dark current correction and significantly increasing radiometric noise. Finally, an attempt was made to identify and mask out remaining outliers in the depth-merged irradiance profiles. This was done by applying Grubb's test at 5% significance level (Guthrie, 2012) to the residual of a second-order polynomial fit of the logarithmic-transformed spectral irradiance observations for a 2 m depth window, sliding down in steps of 1 m. While this procedure has successfully identified individual spikes, some obvious outliers extending over several depth bins remain in the merged dataset, and users will need to make their own judgment on how to identify and remove those. Examples of depth-merged irradiance profiles are shown in Fig. 3 for one clear-water site in the NE Atlantic and one CDOM-rich site in the Baltic Sea.

Note that extrapolated surface values and depth-merged profiles for a specific site are not necessarily derived from the same observations. This is especially true for helicopter-based operations typically comprising several up- and downcast close to the water surface to increase the likelihood of having sufficient observations for the surface extrapolation, while usually only one or two deep-water casts were made to obtain observations at larger depth. The best-suited observations for surface extrapolation do therefore not necessarily correspond to the cast used for depth merging.

#### 2.4.4 Profiles of the diffuse attenuation coefficient

Downward ( $K_{Ed}$ ,  $m^{-1}$ ) and upward ( $K_{Eu}$ ,  $m^{-1}$ ) spectral diffuse attenuation coefficients have been derived from the depth-merged irradiance data by fitting an exponential function through the irradiance observations within a 2 m depth window, sliding down in steps of 0.2 m. The calculation was only performed if at least five observations were available within each bin. The choice of the binning window width was based on a compromise between two conflicting requirements. On the one hand, the window width should be small enough to allow resolving relatively narrow vertical features, such as for example a deep chlorophyll  $a$  maximum. On the other hand, it should be wide enough to allow for an accurate estimation of  $K$ . This relatively narrow window width favors vertical resolution over accuracy: while even relatively narrow vertical features remain visible in the derived  $K$  profiles, these are on the other hand affected by remaining outliers, instrument tilt variations, or instrumental noise. Obviously, users may use the depth-merged irradiance profiles to derive  $K$  profiles or depth-integrated  $K$  values to better meet their individual requirements.

#### 2.4.5 Chromophoric dissolved organic matter (laboratory measurements)

Measurements of chromophoric dissolved organic matter (CDOM) absorption ( $a_{CDOM}$ ,  $m^{-1}$ ) were performed in the laboratory using a spectrophotometer (Perkin Elmer, Lambda 12) on water samples filtered on a 0.22  $\mu m$  Millipore membrane pre-rinsed with 50 ml of Milli-Q water (Babin, 2003).  $a_{CDOM}$  spectra were measured between either 300-750 nm or 350-750 nm at 1-nm increment.

#### 2.4.6 Particulate, non-algal and phytoplankton absorption (laboratory measurements)

Water samples were filtered onto 25 mm glass fiber filters (Whatman, GF/F) at a low vacuum before absorption measurement (Babin, 2003). Total particulate absorption ( $a_p$ ,  $m^{-1}$ ) was measured on particles retained on the filters between 380 and 750 nm



at 1-nm increment using a spectrophotometer equipped with a 60 mm integrating sphere (Perkin Elmer, Lambda 19), and following the transmittance-reflectance (TR) method (Tassan and Ferrari, 1995, 1998). Afterward, pigments were removed from the particles with sodium-hypochloride to measure non-algal (or non-pigmented) absorption ( $a_{NAP}$ ,  $m^{-1}$ ). Finally, phytoplankton absorption ( $a_{\phi}$ ,  $m^{-1}$ ) was retrieved by subtracting  $a_{NAP}$  from  $a_P$ .  $a_{CDOM}$  and  $a_{NAP}$  absorption spectra were fitted according to the following equation (Jerlov, 1968; Bricaud et al., 1981):

$$a_{\tau}(\lambda) = a_{\tau}(\lambda_0)e^{-S_{\tau}(\lambda-\lambda_0)} + k \quad (3)$$

Where  $a_{\tau}$  is the absorption coefficient, either  $a_{CDOM}$  or  $a_{NAP}$  ( $m^{-1}$ ),  $\lambda$  is the wavelength (nm),  $\lambda_0$  is a reference wavelength (443 nm),  $S_{\tau}$  is the spectral slope ( $nm^{-1}$ ) that describes the approximate exponential decrease in absorption with increasing wavelength and  $k$  a background constant ( $m^{-1}$ ) accounting for scatter in the cuvette and drift of the instrument.  $a_{CDOM}$  spectra were fitted using observations below 700 nm, whereas  $a_{NAP}$  fits were performed between 380 and 730 nm, excluding spectral regions between 400-480 nm and 620-710 nm to avoid possible residual pigment absorption (Babin, 2003).  $a_{CDOM}$  and  $a_{NAP}$  were baseline corrected by subtracting the background parameter ( $k$ ) derived from the following equation:

$$\hat{a}_{\tau}(\lambda) = a_{\tau}(\lambda) - k \quad (4)$$

Finally, the spectral background of  $a_P$  spectra (i.e., the average absorption measured between 746 and 750 nm) were added to  $a_{NAP}$ . The underlying rationale is that absorption by phytoplankton in the near-infrared (NIR) is null, and that absorption measured in the NIR for total particles using the TR method is real (Tassan and Ferrari, 2003) and belongs exclusively to non-algal particles. The absorption signal measured for total particles retained on untreated filters is assumed more reliable than that measurement on bleached filters.

#### 2.4.7 Total absorption and scattering (in situ measurements)

In situ vertical profiles of absorption ( $a$ ,  $m^{-1}$ ) and beam attenuation ( $c$ ,  $m^{-1}$ ) were acquired at nine wavelengths (412, 440, 488, 510, 555, 630, 532 or 650 depending on instrument configuration, 676, and 715 nm) using a flow-through in situ absorbance-attenuance meter (AC9, Wetlabs). As the measurements are referenced to pure (Milli-Q) water, the obtained absorption and attenuation coefficients exclude the contribution of water. To correct absorption measurements for incomplete recovery of scattered light,  $a(715)$  was subtracted from  $a(\lambda \leq 715)$ . Scattering coefficients ( $b$ ,  $m^{-1}$ ), were calculated by subtracting absorption from attenuation. As the contribution of molecular (water) scattering is excluded (see above), this coefficient essentially corresponds to particle scattering and is hereafter denoted  $b_P$  ( $m^{-1}$ ).

### 3 Data quality control and data processing

Different general quality control procedures were adopted to ensure the integrity of the data. First, the raw data were visualized and screened to eliminate errors both originating from the measurement devices, including sensors (systematic or random),





and errors inherent to measurement procedures and methods. Statistical metrics such as average, standard deviation, and range were computed to detect and remove anomalous values in the data. Then, data were checked for duplicates and remaining outliers. The complete list of variables is presented in Table 1.

#### 4 Data description (an overview)

##### 210 4.1 Spatial variability along the coastal-ocean gradient

The COAST $\ell$ OOC sampling strategy was primarily designed to capture the bio-optical gradient across the sampled ecosystems and along transects from the coast towards the open ocean within each area (Fig. 1). The following sections present an overview of a few selected variables measured in the different areas. An extensive and detailed explanatory visualization analysis is presented in the final report of the COAST $\ell$ OOC project (Aiken et al., 2023).

##### 215 4.1.1 chlorophyll *a* and particulate organic carbon

As observed in Fig. 4, both total chlorophyll *a* and particulate organic carbon (POC) concentrations varied markedly across the sampled areas, reflecting the natural gradient captured by the sampling strategy. Across all the stations, total chlorophyll *a* ranged between 0.05 and 29 mg m<sup>-3</sup>. The median chlorophyll *a* ranged between 0.1 mg m<sup>-3</sup> in the Atlantic Ocean and 5.9 mg m<sup>-3</sup> in the Baltic Sea (Fig. 4A). Based on the definition proposed by Antoine et al. 1996, the sampled stations were representative of a wide range of trophic status: oligotrophic ( $n = 17$ , chlorophyll *a*  $\leq 0.1$  mg m<sup>-3</sup>), mesotrophic ( $n = 106$ ,  $0.1 \leq$  chlorophyll *a*  $\leq 1$  mg m<sup>-3</sup>) and eutrophic ( $n = 245$ , chlorophyll *a*  $> 1$  mg m<sup>-3</sup>). A similar shore-to-sea gradient pattern could be observed for POC, with median values varying between 0.1 g m<sup>-3</sup> and 0.8 g m<sup>-3</sup> in the Mediterranean Sea (case 2) and Baltic Sea, respectively (Fig. 4B, range between 0.02 and 2.5 g m<sup>-3</sup>).

##### 4.1.2 Inherent optical properties (IOPs)

225 Average absorption spectra by area for total particulate ( $a_P$ ), non-algal particles ( $a_{NAP}$ ), phytoplankton ( $a_\phi$ ), and chromophoric dissolved organic matter ( $a_{CDOM}$ ) are presented in Fig. 5. Phytoplankton maximum absorption peaks, at around 440 nm and 675 nm, are easily distinguishable in Fig. 5C and were found to be highly correlated with the concentration of total chlorophyll *a* (Pearson's  $r > 0.90$ ). Across all the areas,  $a_{CDOM}(350)$ , a proxy for water color and dissolved carbon concentration, varied between 0.03 and 3.66 m<sup>-1</sup>. These values fall within the ranges of the mean values reported globally in the ocean (0.14 m<sup>-1</sup>), 230 coastal (1.82 m<sup>-1</sup>), and estuaries (4.11 m<sup>-1</sup>) ecosystems (Massicotte et al., 2017). Overall, the highest absorption by dissolved organic matter was observed in the Baltic Sea (Fig. 5D). Sampled stations in this area were located West of the Oder River plume, which drains important quantities of humic substance from its catchment area. In contrast, the lowest CDOM absorption was observed in the Atlantic Ocean, where stations were located away from land and thus less influenced by terrestrial inputs (Fig. 1). The spatial variability of CDOM is further strengthened in Fig. 5E, where  $a_{CDOM}(350)$  decreased by a factor of four





235 between the two most distanced points (approximately 40 km) of the westernmost transect sampled in the North Sea (see Fig. 1B).

Light scattering by suspended particles in the water column is a driver of reflectance variability and is often used by remote sensing applications to discriminate between Case 1 and Case 2 waters (Sat, 2000; Morel and Bélanger, 2006). The particulate scattering coefficient at 440 nm,  $b_p(440)$  ranged between  $0.05 \text{ m}^{-1}$  and  $35.8 \text{ m}^{-1}$  (Fig. 6A). The median values varied by almost  
240 two orders of magnitude between the Atlantic Ocean and the Adriatic Sea (Fig. 6A). Furthermore,  $b_p(440)$  showed more or less the same spatial pattern as the downward irradiance attenuation coefficient at 440 nm,  $K_{Ed}(443)$ , which median values varied between  $0.05 \text{ m}^{-1}$  and  $1.21 \text{ m}^{-1}$  in the Atlantic Ocean and the North Sea respectively (Fig. 6B, Pearson's  $r = 0.76$ ).

### 4.1.3 Apparent optical properties (AOPs)

Subsurface reflectance  $R(0^-)$  for all COAST $\ell$ OOC sites is shown in Fig. 7, reflecting the fundamental differences in the bio-  
245 optical properties of the different areas visited. For example, due to enhanced CDOM absorption, reflectance in the blue part of the spectrum is generally low at the Baltic Sea sites, while it is higher in the Case-1 waters encountered in the Atlantic Ocean or the Mediterranean Sea. In the red and NIR, very high reflectance values are observed in the sediment rich waters of the North Sea or the English Channel.

Sample profiles of the diffuse attenuation coefficient  $K_{Ed}(490)$  at a vertical resolution between 2.0 and 5.0 m are shown in  
250 Fig. 8 for two transition zones, each ranging from turbid waters close to the coast to clearer waters further offshore. Fig. 8A shows  $K_{Ed}(490)$  values along a transect taken in the Lion's Gulf on 30. Sept. 1997 from site C4014 located ca. 5 km to the west of the mouth of the main Rhône branch (Grand Rhône) to site C4019 some 20 km further south in clear Mediterranean waters. While  $K_{Ed}(490)$  at the offshore sites C4017 to C4019 adopts low values between ca.  $0.02$  and  $0.05 \text{ m}^{-1}$  reflecting clear-water conditions, sites C4014 and C4015 are strongly influenced by the Rhône river plume, resulting in  $K_{Ed}(490)$  reaching values of  
255 up to  $0.8 \text{ m}^{-1}$  in the surface layer. The turbid Rhône freshwater is floating on top of much denser and clearer Mediterranean seawater, resulting in a strong stratification. Fig. 8B shows a similar transect taken in the North Sea on 12. Sept. 1998 extending from site C6063 close to the western shore of the island of Texel to site C6069 located ca. 22 km further west in the open North Sea. Again, there is a distance-to-coast-dependent decrease of  $K_{Ed}(490)$  values likely related to turbidity, from ca.  $0.8$  to  $1.0 \text{ m}^{-1}$  close to the coast down to values of ca.  $0.2$  to  $0.3 \text{ m}^{-1}$  offshore. In contrast to the transect in the Lion's Gulf, there is no  
260 obvious stratification.  $K_{Ed}(490)$  values are rather homogeneous over the entire water column, pointing to effective mixing.

## 4.2 Co-variability across bio-optical measurements

Few research papers have previously shown how optically significant components and AOPs/IOPs measured during the COAST $\ell$ OOC missions co-varied (Ferrari, 2000; Ferrari et al., 2003; Babin, 2003; Babin et al., 2003). In this section, a brief overview of selected pairwise relationships is presented. Figure 4 shows that total chlorophyll  $a$  co-varied with POC, and Fig. 9A shows  
265 that this relationship is highly variable across the area. Whereas the global Pearson's correlation is  $0.79$  ( $n = 299$ ), it ranged between  $0.36$  in the North Sea ( $n = 88$ ) to  $0.78$  in the Adriatic Sea ( $n = 37$ ) showing that optically significant components do not necessarily covary altogether. Likewise, the global Pearson's correlation between  $a_\phi$  and total chlorophyll  $a$  (Fig. 9B) was



relatively high ( $r = 0.9$ ,  $n = 338$ ). The lowest and highest correlations were observed in the North Sea ( $r = 0.69$ ,  $n = 88$ ) and the Adriatic Sea ( $r = 0.91$ ,  $n = 38$ ), respectively. POC concentration is well known to be an important driver of both IOPs and AOPs in aquatic ecosystems (Stramski et al., 2008; Cetinić et al., 2012). Unsurprisingly, positive correlations were observed between POC and  $K_{Ed}$ (443) (Fig. 9C,  $r = 0.81$ ,  $n = 204$ ) and  $b_p$ (440) (Fig. 9D,  $r = 0.67$ ,  $n = 165$ ).

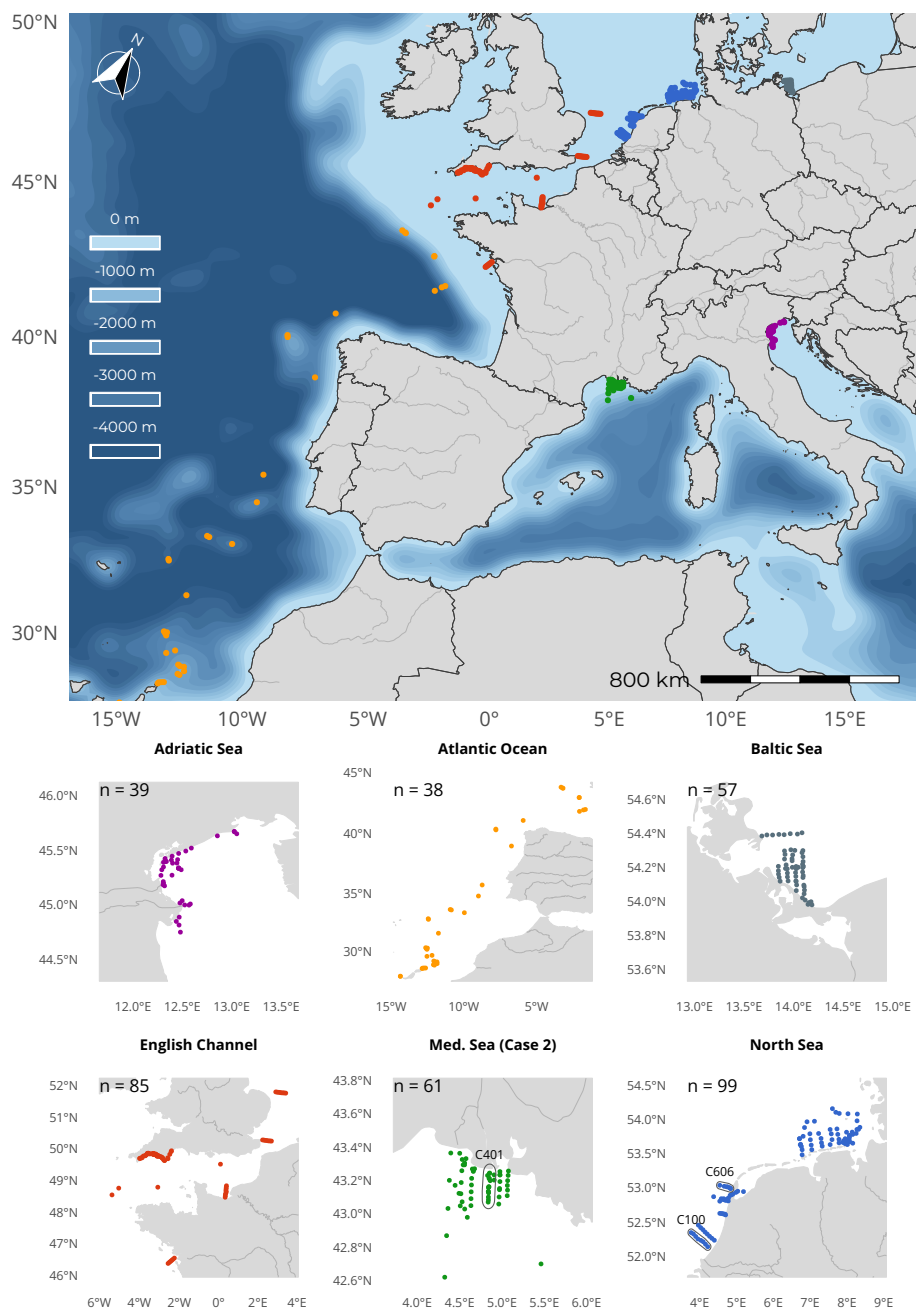
Based on the size-reactivity continuum model proposed by Benner and Amon 2015, physicochemical and photochemical processes are shaping the size distribution of organic matter along the aquatic continuum, and determine the contrasted intrinsic nature of the particles for each type of ecosystem. This is likely one key reason explaining why the observed relationships are quite variable across the different sampled ecosystems (Fig. 9). For example, in coastal areas (e.g., Baltic Sea, Fig. 1), the POC content is generally influenced by large humic organic particles drained by rivers from the surrounding watershed (Babin et al., 2003). Consequently, in these areas, POC concentration (Fig. 4B), absorption (Fig. 5), and downward attenuation coefficients (Fig. 9C) were higher than in other sampled areas. In contrast, the stations that were farther away from the coast (such as the Atlantic Sea, Fig. 1) had lower POC concentrations (Fig. 4B) and absorption (Fig. 5). This is suggesting that the particulate pool was typically made up of smaller, less colored molecules that were mostly made by primary production in situ.

## 5 Code and data availability

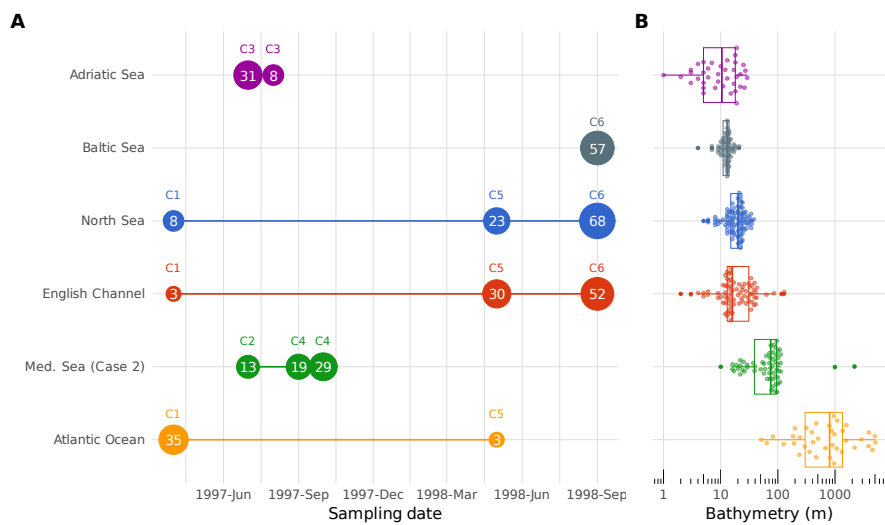
The COASTLOOC data is provided as a collection of comma-separated values (CSV) files that are regrouping measurements associated with a particular type of measure. To aid the user to merge these files, there is a lookup table file called stations.csv that can serve as a table to join the data together based on the station's unique identifier. Table 1 shows the complete list of available measurements and their associated principal investigators. The processed and tidied version of the data is hosted at SEANOIE (SEA scieNtific Open data Edition) under the CC-BY license (<https://www.seanoie.org/data/00824/93570/>, Massicotte et al. 2023). All statistical analyses were performed in R version 4.2.2 (R Core Team, 2022). The code used to produce the figures and the analysis presented in this paper is available under the GNU GPLv3 license (10.5281/zenodo.7708653, Massicotte 2023).

## 6 Conclusions

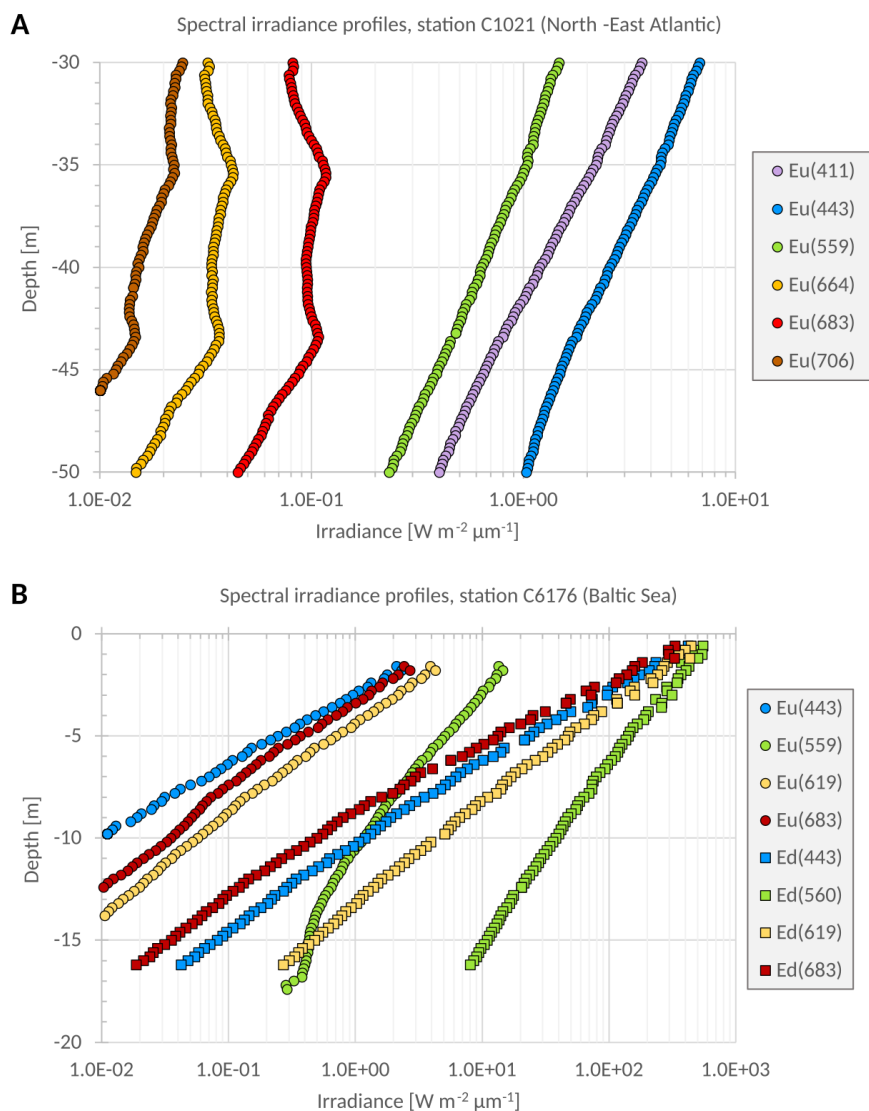
The consolidated, quality-controlled, data collected during the COASTLOOC oceanographic expeditions offer, even if collected more than twenty years ago, many possibilities to better understand the bio-optical dynamics along the land-to-sea gradient where optically-complex water drained from watersheds mix with seawater. In this paper, only a subset of variables has been presented. The reader is referred to Table 1 for a complete list and description of variables collected during the COASTLOOC expeditions.




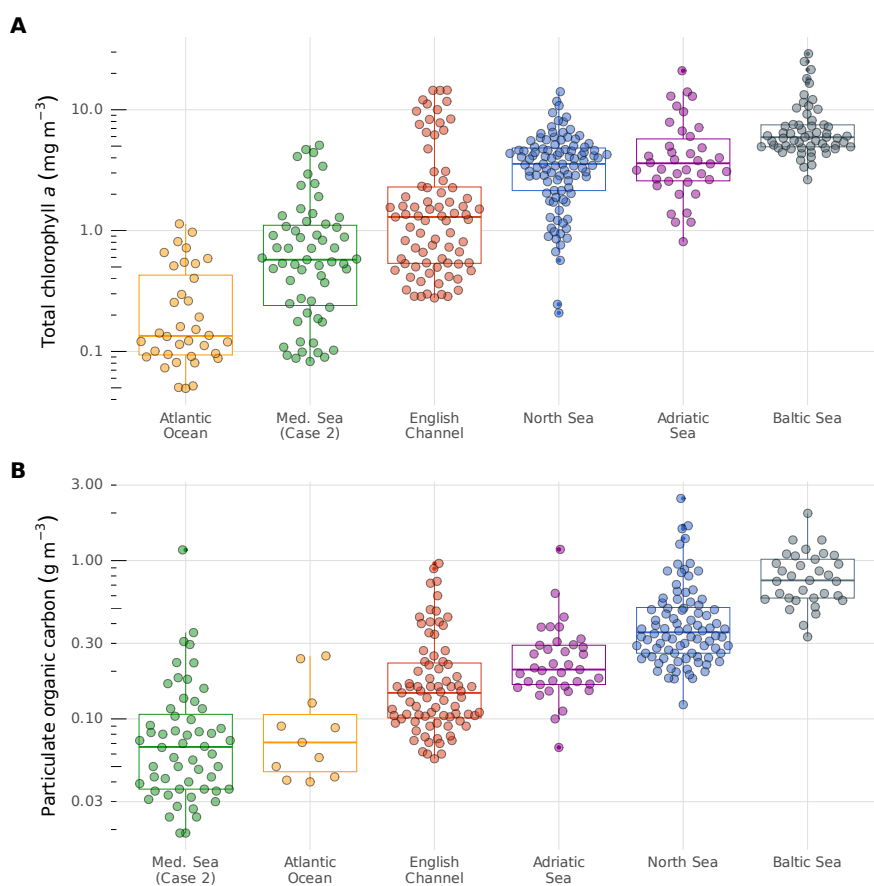
**Figure 1.** Map of the sampling stations. The three black outlines in the bottom panels (Mediterranean Sea and North Sea) identify the stations and the transects used in Fig. 5E (C100) as well as for the examples of vertical profiles of  $K_{Ed}(490)$  in Fig. 8 (C401 and C606).



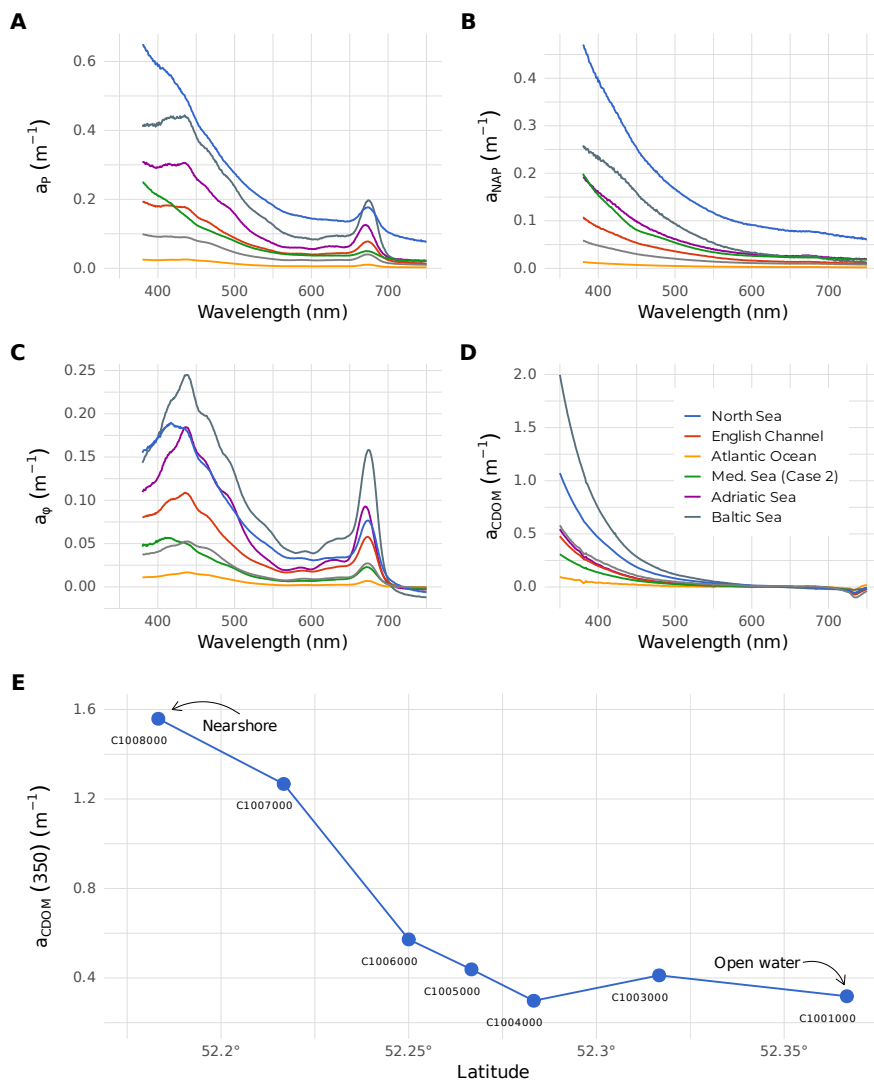
**Figure 2.** (A) Overview of the temporal sampling for the six areas. The numbers in the circles indicate the number of visited stations each month. (B) Boxplot showing the bathymetry at the sampling locations by area. The labels on top of each circle identify the COAST/OOC campaigns (C1 to C6).



**Figure 3.** (A) Vertical profile of the upwelling irradiance taken on 11 April 1997 at station C1021 located in the North-East Atlantic offshore Northern Portugal. A double deep chlorophyll maximum with the corresponding irradiance increase due to chlorophyll fluorescence is observed at water depths of ca. 35 m at  m, most prominently at 683 nm, but also at 664 nm and even at 706 nm. Attenuation in the blue to green wavelengths is correspondingly enhanced as reflected by the change in slope at a depth of ca. 34 m. (B) Vertical profiles of the upwelling and downwelling irradiance taken on 25 September 1998 at station C6176 located in the Baltic Sea offshore Usedom Island in North-East Germany. Baltic Sea waters are rich in CDOM, resulting in strong absorption in the UV and blue. The reduced decrease of the upwelling irradiance at 559 nm towards larger depths is likely caused by reflection of downwelling irradiance from the ocean bottom. Chlorophyll fluorescence is likely the reason for the relatively enhanced upwelling irradiance at 683 nm for depths below ca. 7 m.

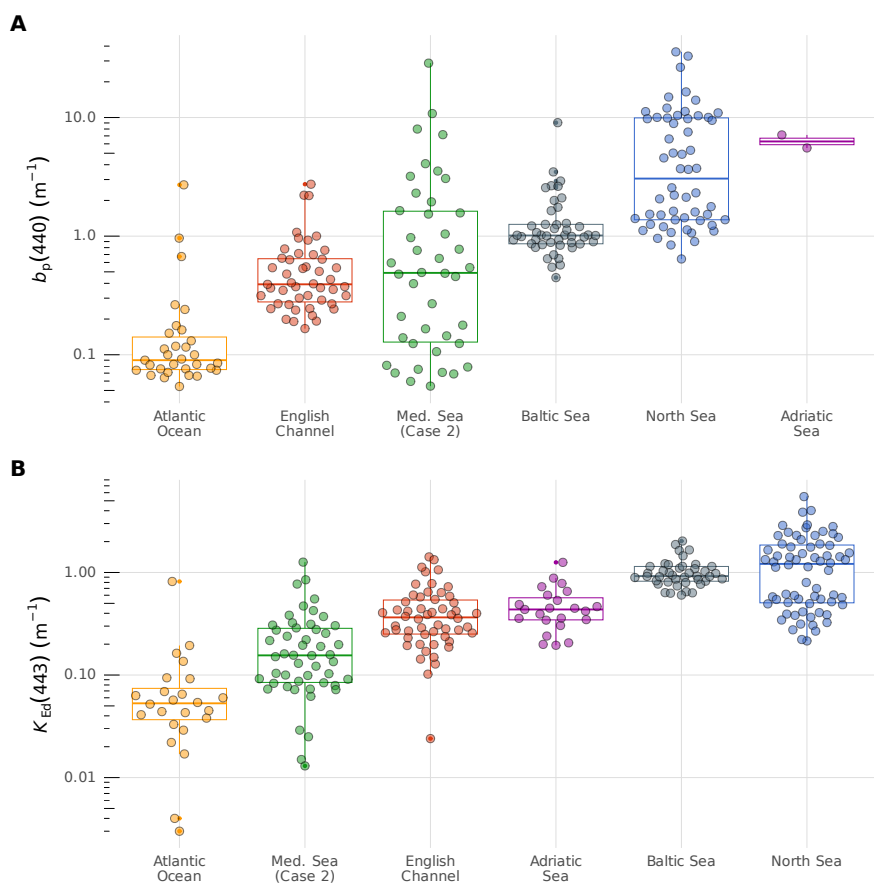


**Figure 4.** (A) Total chlorophyll *a* and (B) particulate organic carbon across the sampled areas.

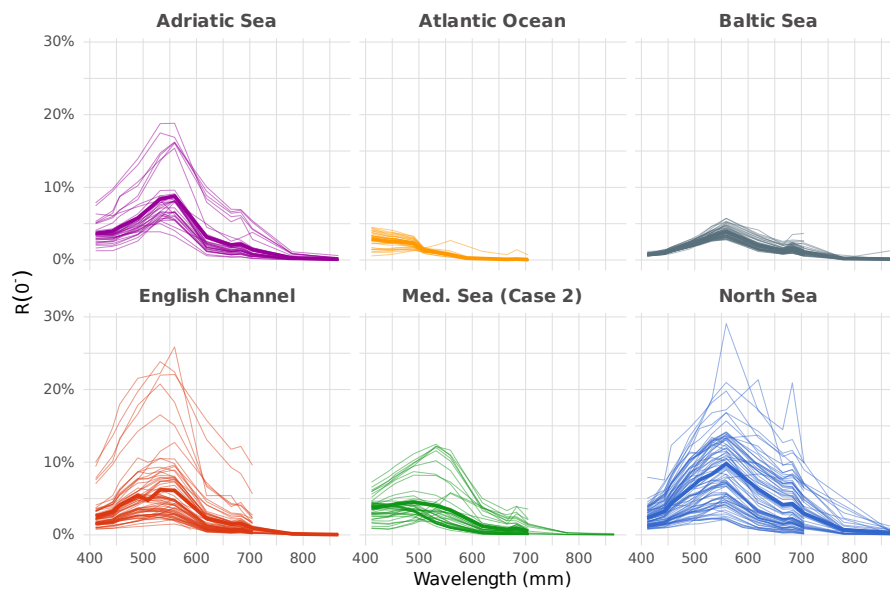


**Figure 5.** (A) Average total particulate ( $a_p$ ), (B) non-algal ( $a_{NAP}$ ), (C) phytoplankton ( $a_\phi$ ) and (D) chromophoric dissolved organic matter ( $a_{CDOM}$ ) absorption spectra in each area. (E)  $a_{CDOM}(350)$  along the westernmost transect in the North Sea (see Fig. 1B).

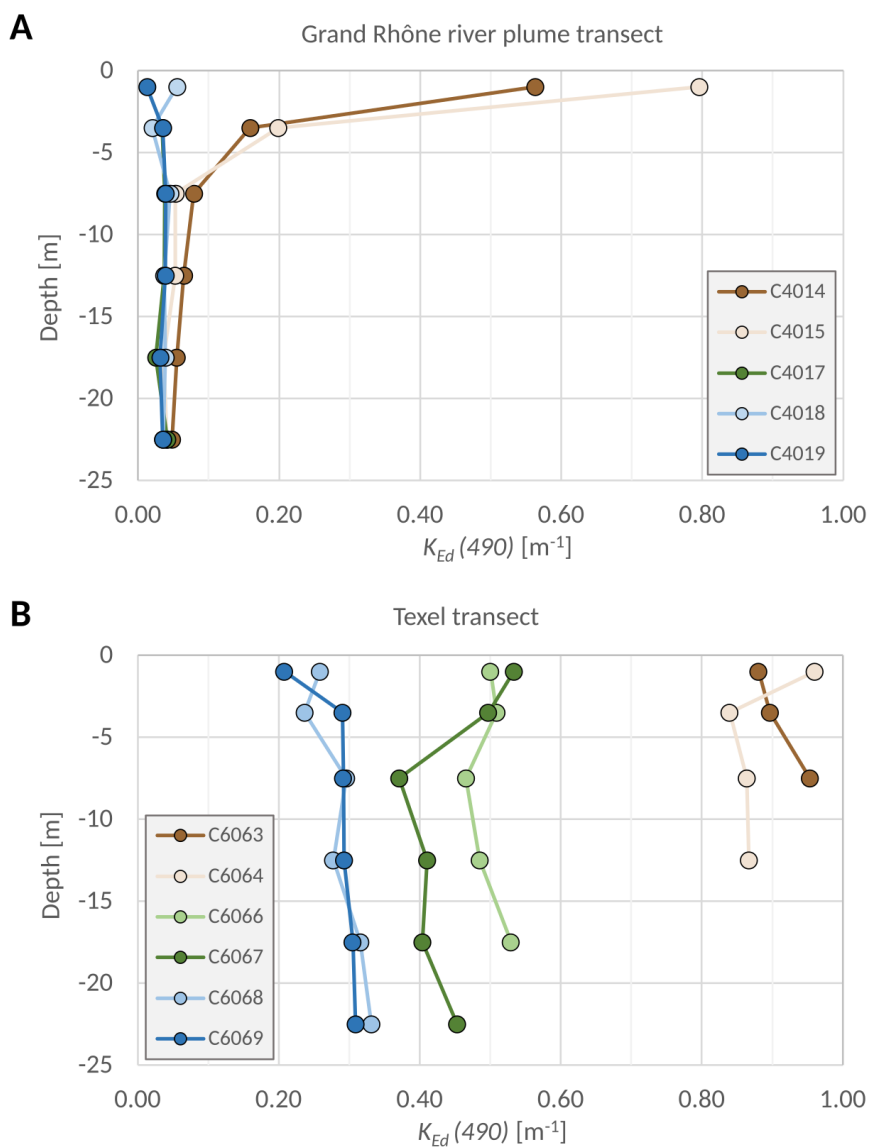




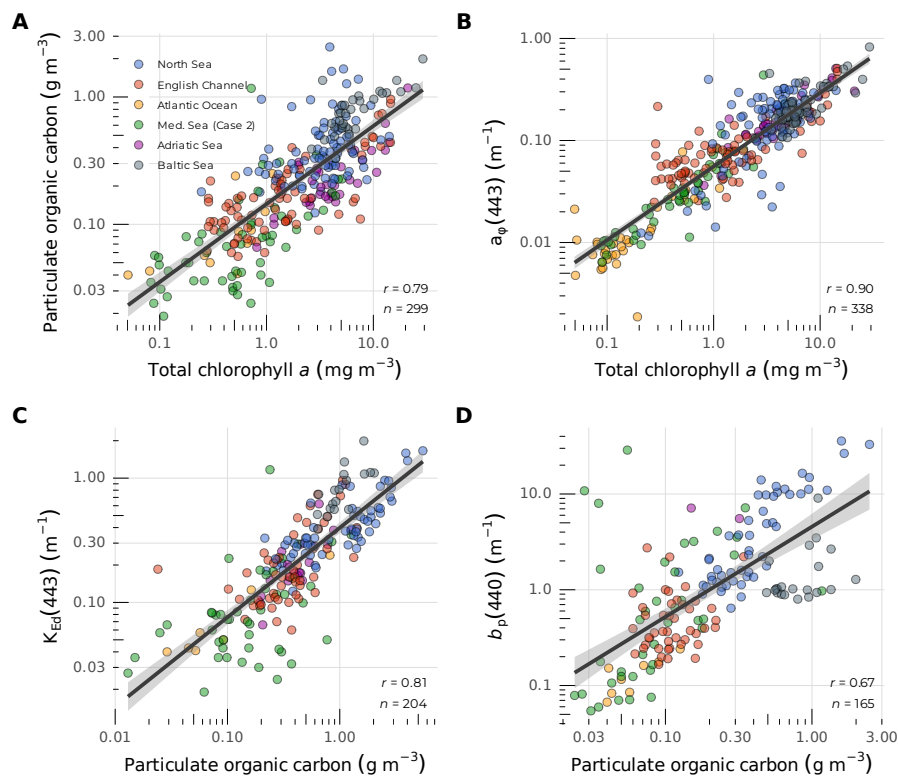
**Figure 6.** (A) Particulate scattering coefficient at 440 nm ( $b_p(440)$ ) and (B) attenuation coefficient for downward irradiance at 443 nm ( $K_{Ed}(443)$ ) across the sampled areas.



**Figure 7.** Subsurface reflectance  $R(0^-)$  across the sampled areas. The thick lines represent the regional averages. Note that  $R(0^-)$  at wavelengths above 705 nm could only be derived from helicopter-based measurements.



**Figure 8.** (A)  $K_{Ed}(490)$  profiles taken in the Lion's Gulf on 30. Sept. 1997 along a transect extending from site C4014 located ca. 5 km to the west of the mouth of the main Rhône branch (Grand Rhône) to site C4019 located some 20 km further south in clear Mediterranean waters. (B)  $K_{Ed}(490)$  profiles taken in the North Sea on 12. Sept 1998 along a transect extending from site C6063 close to the western shore of the island of Texel to site C6069 located ca. 22 km further west in the open North Sea.



**Figure 9.** Scatterplots showing relationships among different selected variables. (A) Particulate organic carbon (POC) and (B) phytoplankton absorption at 443 nm ( $a_p(443)$ ) against total chlorophyll \*a\*. (C) Downward irradiance at 443 nm ( $K_{Ed}(443)$ ) and (D) particulate scattering at 440 nm ( $b_p(440)$ ) against particulate organic carbon. The red lines show the linear relationships between the variables. The shaded gray areas represent the 95% confidence intervals around the fitted models.

Table 1: List of measured parameters

| Source file    | Variable           | Units           | Description   |
|----------------|--------------------|-----------------|---|
| absorption.csv | wavelength         | nm              |   |
| absorption.csv | a_p_m1             | m <sup>-1</sup> | Total particulate absorption  |
| absorption.csv | a_nap_m1           | m <sup>-1</sup> | Non-algal absorption  |
| absorption.csv | a_nap_adjusted_m1  | m <sup>-1</sup> | Non-algal absorption adjusted for...  |
| absorption.csv | a_cdom_m1          | m <sup>-1</sup> | Chromophoric dissolved organig matter absorption                                  |
| absorption.csv | a_cdom_adjusted_m1 | m <sup>-1</sup> | Chromophoric dissolved organig matter absorption with background baseline removed |



Table 1: List of measured parameters (*continued*)

| Source file         | Variable                     | Units                              | Description   |
|---------------------|------------------------------|------------------------------------|---|
| absorption.csv      | a_phy_m1                     | m <sup>-1</sup>                    | Phytoplankton absorption  |
| absorption.csv      | background_a_p_m1            |                                    | Baseline background of total particulate absorption   |
| absorption.csv      | background_a_cdom_m1         |                                    | Baseline background of chromophoric dissolved organic matter absorption                           |
| absorption.csv      | background_a_nap_m1          |                                    | Baseline background of non-algal absorption   |
| ac9.csv             | a_m1                         | m <sup>-1</sup>                    | Total non-water absorption coefficient  |
| ac9.csv             | c_m1                         | m <sup>-1</sup>                    | Total non-water attenuation coefficient   |
| ac9.csv             | bp_m1                        | m <sup>-1</sup>                    | Particle scattering coefficient   |
| bathymetry.csv      | longitude                    | Degree decimal                     | Longitude of the pixel used to extract the bathymetry   |
| bathymetry.csv      | latitude                     | Degree decimal                     | Latitude of the pixel used to extract the bathymetry  |
| bathymetry.csv      | bathymetry_m                 | m                                  | Bathymetry depth at the sampled stations  |
| irradiance.csv      | eu_w_m2_um                   | w m <sup>-2</sup> μm <sup>-1</sup> | Upward irradiance just beneath the water surface (Eu0-)   |
| irradiance.csv      | ed_w_m2_um                   | w m <sup>-2</sup> μm <sup>-1</sup> | Downward irradiance just beneath the water surface (Ed0-)   |
| irradiance.csv      | k_eu_m1                      | m <sup>-1</sup>                    | Attenuation coefficient for upward irradiance (just beneath the water surface)                    |
| irradiance.csv      | k_ed_m1                      | m <sup>-1</sup>                    | Attenuation coefficient for downward irradiance (just beneath the water surface)                  |
| reflectance.csv     | measured_reflectance_percent | Percent                            | Surface water reflectance   |
| spectral_slopes.csv | s_cdom_nm1                   | nm <sup>-1</sup>                   | Spectral slope that describes the approximate exponential decrease in aCDOM                       |
| spectral_slopes.csv | s_nap_nm1                    | nm <sup>-1</sup>                   | Spectral slope that describes the approximate exponential decrease in aNAP                        |
| spectral_slopes.csv | a_cdom443_m1                 | m <sup>-1</sup>                    |   |
| spectral_slopes.csv | a_nap443_m1                  | m <sup>-1</sup>                    |   |
| stations.csv        | station                      |                                    | Unique ID of the sampled station. Can be used as unique key to merge the data across other files. |
| stations.csv        | date                         |                                    | Date at which the measurement was made  |
| stations.csv        | depth_m                      | m                                  | Depth at which the measurement was made   |
| stations.csv        | longitude                    | Degree decimal                     | Longitude of the sampling station   |
| stations.csv        | latitude                     | Degree decimal                     | Latitude of the sampling station  |



Table 1: List of measured parameters (*continued*)

| Source file  | Variable                          | Units              | Description  |
|--------------|-----------------------------------|--------------------|--|
| stations.csv | area                              |                    | Region where the measurement was made. One of: (1) North Sea, (2) English Channel, (3) Atlantic Ocean, (4) Med. Sea (Case 2), (5) Adriatic Sea, (6) Baltic Sea |
| stations.csv | system                            |                    |  |
| stations.csv | gmt_time                          |                    |  |
| stations.csv | solar_zenith_angle                | degree             | Angle of the sun from the vertical   |
| pigments.csv | chlorophyll_a_mg_m3               | mg m <sup>-3</sup> | Chlorophyll-a  |
| pigments.csv | chlorophyll_b_mg_m3               | mg m <sup>-3</sup> | Chlorophyll-b  |
| pigments.csv | chlorophyll_c_mg_m3               | mg m <sup>-3</sup> | Chlorophyll-c  |
| pigments.csv | pheopigment_mg_m3                 | mg m <sup>-3</sup> | Pheopigment  |
| pigments.csv | fucoxanthin_mg_m3                 | mg m <sup>-3</sup> | Fucoxanthin  |
| pigments.csv | hexanoyloxyfucoxanthin_19_mg_m3   | mg m <sup>-3</sup> | Hexanoyloxyfucoxanthin-19  |
| pigments.csv | butanoyloxyfucoxanthin_19_mg_m3   | mg m <sup>-3</sup> | Butanoyloxyfucoxanthin-19  |
| pigments.csv | alloxanthin_mg_m3                 | mg m <sup>-3</sup> | Alloxanthin  |
| pigments.csv | zeaxanthin_mg_m3                  | mg m <sup>-3</sup> | Zeaxanthin   |
| pigments.csv | prasixanthin_mg_m3                | mg m <sup>-3</sup> | Prasixanthin   |
| pigments.csv | neoxanthin_mg_m3                  | mg m <sup>-3</sup> | Neoxanthin   |
| pigments.csv | violaxanthin_mg_m3                | mg m <sup>-3</sup> | Violaxanthin   |
| pigments.csv | diatoxanthin_mg_m3                | mg m <sup>-3</sup> | Diatoxanthin   |
| pigments.csv | diadinoxanthin_mg_m3              | mg m <sup>-3</sup> | Diadinoxanthin   |
| pigments.csv | peridinin_mg_m3                   | mg m <sup>-3</sup> | Peridinin  |
| pigments.csv | carotene_mg_m3                    | mg m <sup>-3</sup> | Carotene   |
| pigments.csv | lutein_mg_m3                      | mg m <sup>-3</sup> | Lutein   |
| carbon.csv   | suspended_particulate_matter_g_m3 | g m <sup>-3</sup>  | Suspended particulate matter   |
| carbon.csv   | particulate_organic_nitrogen_g_m3 | g m <sup>-3</sup>  | Particulate organic nitrogen   |
| carbon.csv   | total_particulate_carbon_g_m3     | g m <sup>-3</sup>  | Total particulate carbon   |
| carbon.csv   | particulate_organic_carbon_g_m3   | g m <sup>-3</sup>  | Particulate organic carbon   |
| carbon.csv   | dissolved_organic_carbon_g_m3     | g m <sup>-3</sup>  | Dissolved organic carbon   |
| SPMR         | Cast                              | 1                  | Processed cast number  |



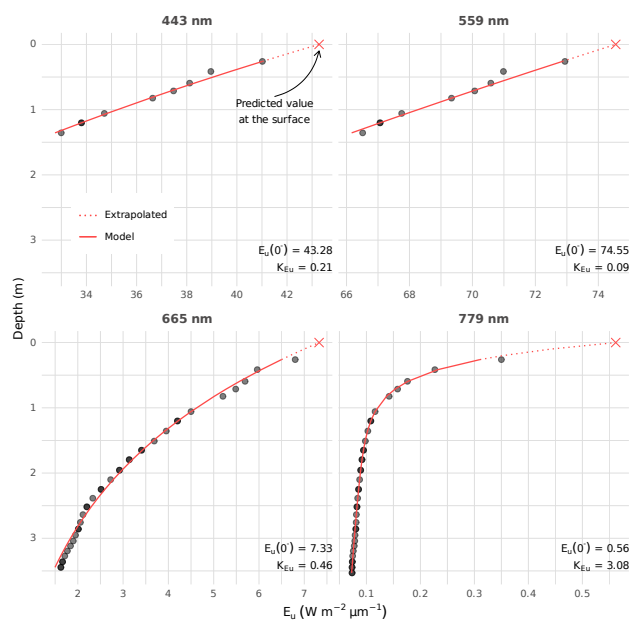
Table 1: List of measured parameters (*continued*)

| Source file | Variable | Units                                | Description  |
|-------------|----------|--------------------------------------|--|
| SPMR        | Depth    | m                                    | Depth of vertical bin, e.g. -1.00 representing the depth bin [-0.90, -1.10 m]    |
| SPMR        | TmpWat   | Degree celcius                       | Water temperature  |
| SPMR        | Cond     | ms cm <sup>-1</sup>                  | Conductivity   |
| SPMR        | Salin    | PSU                                  | Salinity   |
| SPMR        | SigmaT   | 1                                    | Density of sea water   |
| SPMR        | TiProf   | Degree                               | Tilt of profiling radiometer   |
| SPMR        | TiRef    | Degree                               | Tilt of reference radiometer   |
| SPMR        | VSpeed   | m s <sup>-1</sup>                    | Vertical speed   |
| SPMR        | Altim    | m                                    | Altimeter sounding of distance from the ocean ground                             |
| SPMR        | N_OBS    | 1                                    | Number of observations within depth bin  |
| SPMR        | EUnnn    | w m <sup>-2</sup> μm <sup>-1</sup>   | In-water upwelling irradiance at wavelength nnn                                  |
| SPMR        | EDnnn    | w m <sup>-2</sup> μm <sup>-1</sup>   | In-water downwelling irradiance at wavelength nnn                                |
| SPMR        | ERnnn    | w m <sup>-2</sup> μm <sup>-1</sup>   | In-air downwelling irradiance at wavelength nnn                                  |
| SPMR        | KUnnn    | m <sup>-1</sup>                      | Diffuse attenuation at wavelength nnn calculated from the upwelling irradiance   |
| SPMR        | KDnnn    | m <sup>-1</sup>                      | Diffuse attenuation at wavelength nnn calculated from the downwelling irradiance |
| SPMR        | PAR_ABS  | μmol m <sup>-2</sup> s <sup>-1</sup> | Phytoplanktonically Active Radiation (PAR)                                       |
| SPMR        | PAR%SRF  | Percent                              | PAR at depth z relative to PAR on the sea surface                                |
| SPMR        | K_PAR    | m <sup>-1</sup>                      | Diffuse attenuation for PAR  |

## Appendix A

### A1





**Figure A1.** Example of extrapolation of the upward irradiance towards the sea surface. The irradiance values just below the sea surface (red crosses,  $E_u(0^-)$ ) and the corresponding diffuse attenuation coefficient for the topmost water layer are specified in the figures. The full lines represent the interpolated values whereas the dashed lines show extrapolation values up to the sea surface.

Table A1: Scientific articles in peer-reviewed journals using or referencing COASTLOOC

| Publications   |
|--|
| Babin, M., Stramski, D., Ferrari, G. M., Claustre, H., Bricaud, A., Obolensky, G., & Hoepffner, N. (2003). Variations in the light absorption coefficients of phytoplankton, nonalgal particles, and dissolved organic matter in coastal waters around Europe. <i>Journal of Geophysical Research: Oceans</i> , 108(C7). |
| Begouen Demeaux, C., & Boss, E. (2022). Validation of Remote-Sensing Algorithms for Diffuse Attenuation of Downward Irradiance Using BGC-Argo Floats. <i>Remote Sens.</i> 2022, 14, 4500.  |
| Belanger, S., Babin, M., & Larouche, P. (2008). An empirical ocean color algorithm for estimating the contribution of chromophoric dissolved organic matter to total light absorption in optically complex waters. <i>Journal of Geophysical Research: Oceans</i> , 113(C4).   |
| Beltrán-Abaunza, J. M., Kratzer, S., & Brockmann, C. (2014). Evaluation of MERIS products from Baltic Sea coastal waters rich in CDOM. <i>Ocean Science</i> , 10(3), 377-396.  |
| Blix, K., Li, J., Massicotte, P., & Matsuoka, A. (2019). Developing a new machine-learning algorithm for estimating chlorophyll-a concentration in optically complex waters: A case study for high northern latitude waters by using Sentinel 3 OLCI. <i>Remote Sensing</i> , 11(18), 2076.                              |
| Caillault, K., Roupioz, L., & Viallefont-Robinet, F. (2021). Modelling of the optical signature of oil slicks at sea for the analysis of multi-and hyperspectral VNIR-SWIR images. <i>Optics Express</i> , 29(12), 18224-18242.  |



Table A1: Scientific articles in peer-reviewed journals using or referencing COASTLOOC (*continued*)

---

Publications

---

Chami, M., & Platel, M. D. (2007). Sensitivity of the retrieval of the inherent optical properties of marine particles in coastal waters to the directional variations and the polarization of the reflectance. *Journal of Geophysical Research: Oceans*, 112(C5).

Claustre, H., Fell, F., Oubelkheir, K., Prieur, L., Sciandra, A., Gentili, B., & Babin, M. (2000). Continuous monitoring of surface optical properties across a geostrophic front: Biogeochemical inferences. *Limnology and Oceanography*, 45(2), 309-321.

D'Alimonte, D., Zibordi, G., Kajiyama, T., & Berthon, J. F. (2014). Comparison between MERIS and regional high-level products in European seas. *Remote sensing of environment*, 140, 378-395.

Defoin-Platel, M., & Chami, M. (2007). How ambiguous is the inverse problem of ocean color in coastal waters?. *Journal of Geophysical Research: Oceans*, 112(C3).

Doerffer, R., & Schiller, H. (2007). The MERIS Case 2 water algorithm. *International Journal of Remote Sensing*, 28(3-4), 517-535.

Doron, M., Babin, M., Mangin, A., & Hembise, O. (2007). Estimation of light penetration, and horizontal and vertical visibility in oceanic and coastal waters from surface reflectance. *Journal of Geophysical Research: Oceans*, 112(C6).

Doron, M., Babin, M., Hembise, O., Mangin, A., & Garnesson, P. (2011). Ocean transparency from space: Validation of algorithms estimating Secchi depth using MERIS, MODIS and SeaWiFS data. *Remote Sensing of Environment*, 115(12), 2986-3001.

Dransfeld, S., Tatnall, A. R., Robinson, I. S., & Mobley, C. D. (2005). Prioritizing ocean colour channels by neural network input reflectance perturbation. *International Journal of Remote Sensing*, 26(5), 1043-1048.

Ferrari, G. M. (2000). The relationship between chromophoric dissolved organic matter and dissolved organic carbon in the European Atlantic coastal area and in the West Mediterranean Sea (Gulf of Lions). *Marine Chemistry*, 70(4), 339-357.

Groom, S., Martinez-Vicente, V., Fishwick, J., Tilstone, G., Moore, G., Smyth, T., & Harbour, D. (2009). The western English Channel observatory: Optical characteristics of station L4. *Journal of Marine Systems*, 77(3), 278-295.

Jamet, C., Loisel, H., & Dessailly, D. (2012). Retrieval of the spectral diffuse attenuation coefficient  $K_d(\lambda)$  in open and coastal ocean waters using a neural network inversion. *Journal of Geophysical Research: Oceans*, 117(C10).

Kratzer, S., & Moore, G. (2018). Inherent optical properties of the baltic sea in comparison to other seas and oceans. *Remote Sensing*, 10(3), 418.

Loisel, H., Stramski, D., Mitchell, B. G., Fell, F., Fournier-Sicre, V., Lemasle, B., & Babin, M. (2001). Comparison of the ocean inherent optical properties obtained from measurements and inverse modeling. *Applied Optics*, 40(15), 2384-2397.

Loisel, H., Vantrepotte, V., Ouillon, S., Ngoc, D. D., Herrmann, M., Tran, V., ... & Van Nguyen, T. (2017). Assessment and analysis of the chlorophyll-a concentration variability over the Vietnamese coastal waters from the MERIS ocean color sensor (2002–2012). *Remote sensing of environment*, 190, 217-232.

Loisel, H., Stramski, D., Dessailly, D., Jamet, C., Li, L., & Reynolds, R. A. (2018). An inverse model for estimating the optical absorption and backscattering coefficients of seawater from remote-sensing reflectance over a broad range of oceanic and coastal marine environments. *Journal of Geophysical Research: Oceans*, 123(3), 2141-2171.

Matsuoka, A., Hill, V., Huot, Y., Babin, M., & Bricaud, A. (2011). Seasonal variability in the light absorption properties of western Arctic waters: Parameterization of the individual components of absorption for ocean color applications. *Journal of Geophysical Research: Oceans*, 116(C2).



Table A1: Scientific articles in peer-reviewed journals using or referencing COASTLOOC (*continued*)

---

Publications

---

Matsuoka, A., Babin, M., Doxaran, D., Hooker, S. B., Mitchell, B. G., Bélanger, S., & Bricaud, A. (2014). A synthesis of light absorption properties of the Arctic Ocean: application to semi-analytical estimates of dissolved organic carbon concentrations from space. *Biogeosciences*, 11(12), 3131-3147.

Morel, A., & Bélanger, S. (2006). Improved detection of turbid waters from ocean color sensors information. *Remote Sensing of Environment*, 102(3-4), 237-249.

Neukermans, G., Loisel, H., Mériaux, X., Astoreca, R., & McKee, D. (2012). In situ variability of mass-specific beam attenuation and backscattering of marine particles with respect to particle size, density, and composition. *Limnology and oceanography*, 57(1), 124-144.

Oubelkheir, K., Claustre, H., Bricaud, A., & Babin, M. (2007). Partitioning total spectral absorption in phytoplankton and colored detrital material contributions. *Limnology and Oceanography: Methods*, 5(11), 384-395.

Schroeder, T., Behnert, I., Schaale, M., Fischer, J., & Doerffer, R. (2007). Atmospheric correction algorithm for MERIS above case-2 waters. *International Journal of Remote Sensing*, 28(7), 1469-1486.

Schroeder, T., Schaale, M., Lovell, J., & Blondeau-Patissier, D. (2022). An ensemble neural network atmospheric correction for Sentinel-3 OLCI over coastal waters providing inherent model uncertainty estimation and sensor noise propagation. *Remote Sensing of Environment*, 270, 112848.

Shahraiyini, T. H., Schaale, M., Fell, F., Fischer, J., Preusker, R., Vatandoust, M., ... & Tavakoli, A. (2007). Application of the Active Learning Method for the estimation of geophysical variables in the Caspian Sea from satellite ocean colour observations. *International Journal of Remote Sensing*, 28(20), 4677-4683.

Tassan, S., Ferrari, G. M., Bricaud, A., & Babin, M. (2000). Variability of the amplification factor of light absorption by filter-retained aquatic particles in the coastal environment. *Journal of Plankton Research*, 22(4), 659-668.

Tassan, S., & Ferrari, G. M. (2002). A sensitivity analysis of the 'Transmittance-Reflectance' method for measuring light absorption by aquatic particles. *Journal of Plankton Research*, 24(8), 757-774.

Wei, J., Wang, M., Jiang, L., Yu, X., Mikelsons, K., & Shen, F. (2021). Global estimation of suspended particulate matter from satellite ocean color imagery. *Journal of Geophysical Research: Oceans*, 126(8), e2021JC017303.

Yu, X., Salama, M. S., Shen, F., & Verhoef, W. (2016). Retrieval of the diffuse attenuation coefficient from GOCI images using the 2SeaColor model: A case study in the Yangtze Estuary. *Remote Sensing of Environment*, 175, 109-119.

Yu, X., Lee, Z., Shen, F., Wang, M., Wei, J., Jiang, L., & Shang, Z. (2019). An empirical algorithm to seamlessly retrieve the concentration of suspended particulate matter from water color across ocean to turbid river mouths. *Remote Sensing of Environment*, 235, 111491.

Zhang, T., Fell, F., Liu, Z. S., Preusker, R., Fischer, J., & He, M. X. (2003). Evaluating the performance of artificial neural network techniques for pigment retrieval from ocean color in Case I waters. *Journal of Geophysical Research: Oceans*, 108(C9).

Zhang, T., & Fell, F. (2004). An approach to improving the retrieval accuracy of oceanic constituents in Case II waters. *Journal of Ocean University of China*, 3(2), 220-224.

Zhang, T., & Fell, F. (2007). An empirical algorithm for determining the diffuse attenuation coefficient  $K_d$  in clear and turbid waters from spectral remote sensing reflectance. *Limnology and Oceanography: Methods*, 5(12), 457-462.



Zheng, G., & Stramski, D. (2013). A model based on stacked-constraints approach for partitioning the light absorption coefficient of seawater into phytoplankton and non-phytoplankton components. *Journal of Geophysical Research: Oceans*, 118(4), 2155-2174.

---

*Author contributions.* Conceptualization: MB, Formal analysis: FF, DD, VSF, MB. Investigation: MB, FF; FF, VFS. Software: DD (AC-9) FF (radiometry), VFS (data acquisition and pre-processing). Writing: PM with support from all co-authors.

300 *Competing interests.* The authors declare no competing interests.

*Acknowledgements.* A great number of people contributed to the generation of the COASTIOOC database as described herein, be it by contributing to project implementation, supporting the field campaigns, performing lab work, or providing scientific guidance. In this respect, we would like especially to thank James Aiken, Jean-François Berthon, Annick Bricaud, Hervé Claustre, Roland Doerffer, Giovanni Massimo Ferrari, Hans Hakvoort, Geir Johnsen, Khadija Oubelkheir, Matt Pinkerton, Rainer Reuter, Marcel Wernand and Grigor Obolensky. We are  
305 also grateful to the crews of the ships (NO Thetis-2, RV Poseidon, RV Victor Hensen) and helicopter (Commerc'Air SA) we used for collecting the field data.



## References

- Remote Sensing of Ocean Colour in Coastal, and Other Optically-Complex, Waters., <https://doi.org/10.25607/OBP-95>, 2000.
- Aiken, J., Antoine, D., Babin, M., Barth, H., Bricaud, A., Chauton, M., Claustre, H., Doerffer, R., Dowell, M., Fell, F., Ferrari, M., Fischer, J., Fournier-Sicre, Vincent, Hakvoort, H., Hoepffner, N., Johnsen, G., Montagner, F., Moore, G., Morel, A., Obolensky, G., Olbert, C., Pinkerton, M., Reuter, R., Sakshaug, E., and Wernand, M.: COASTLOOC (COAstal Surveillance Through Observation of Ocean Colour) Final Report, Tech. rep., Zenodo, <https://doi.org/10.5281/ZENODO.7428384>, 2022.
- Antoine, D., André, J.-M., and Morel, A.: Oceanic Primary Production: 2. Estimation at Global Scale from Satellite (Coastal Zone Color Scanner) Chlorophyll, *Global Biogeochemical Cycles*, 10, 57–69, <https://doi.org/10.1029/95GB02832>, 1996.
- Babin, M.: Variations in the Light Absorption Coefficients of Phytoplankton, Nonalgal Particles, and Dissolved Organic Matter in Coastal Waters around Europe, *Journal of Geophysical Research*, 108, 3211, <https://doi.org/10.1029/2001JC000882>, 2003.
- Babin, M., Morel, A., Fournier-Sicre, V., Fell, F., and Stramski, D.: Light Scattering Properties of Marine Particles in Coastal and Open Ocean Waters Asrelated to the Particle Mass Concentration, *Limnology and Oceanography*, 48, 843–859, <https://doi.org/10.4319/lo.2003.48.2.0843>, 2003.
- Benner, R. and Amon, R. M.: The Size-Reactivity Continuum of Major Bioelements in the Ocean, *Annual Review of Marine Science*, 7, 185–205, <https://doi.org/10.1146/annurev-marine-010213-135126>, 2015.
- Bricaud, A., Morel, A., and Prieur, L.: Absorption by Dissolved Organic Matter of the Sea (Yellow Substance) in the UV and Visible Domains, *Limnology and Oceanography*, 26, 43–53, <https://doi.org/10.4319/lo.1981.26.1.0043>, 1981.
- Carr, M.-E., Friedrichs, M. A., Schmeltz, M., Noguchi Aita, M., Antoine, D., Arrigo, K. R., Asanuma, I., Aumont, O., Barber, R., Behrenfeld, M., Bidigare, R., Buitenhuis, E. T., Campbell, J., Ciotti, A., Dierssen, H., Dowell, M., Dunne, J., Esaias, W., Gentili, B., Gregg, W., Groom, S., Hoepffner, N., Ishizaka, J., Kameda, T., Le Quéré, C., Lohrenz, S., Marra, J., Mélin, F., Moore, K., Morel, A., Reddy, T. E., Ryan, J., Scardi, M., Smyth, T., Turpie, K., Tilstone, G., Waters, K., and Yamanaka, Y.: A Comparison of Global Estimates of Marine Primary Production from Ocean Color, *Deep Sea Research Part II: Topical Studies in Oceanography*, 53, 741–770, <https://doi.org/10.1016/j.dsr2.2006.01.028>, 2006.
- Cetinić, I., Perry, M. J., Briggs, N. T., Kallin, E., D’Asaro, E. A., and Lee, C. M.: Particulate Organic Carbon and Inherent Optical Properties during 2008 North Atlantic Bloom Experiment: POC AND OPTICS-NAB08, *Journal of Geophysical Research: Oceans*, 117, n/a–n/a, <https://doi.org/10.1029/2011JC007771>, 2012.
- Cole, J. J., Prairie, Y. T., Caraco, N. F., McDowell, W. H., Tranvik, L. J., Striegl, R. G., Duarte, C. M., Kortelainen, P., Downing, J. A., Middelburg, J. J., and Melack, J.: Plumbing the Global Carbon Cycle: Integrating Inland Waters into the Terrestrial Carbon Budget, *Ecosystems*, 10, 172–185, <https://doi.org/10.1007/s10021-006-9013-8>, 2007.
- Ferrari, G. M.: The Relationship between Chromophoric Dissolved Organic Matter and Dissolved Organic Carbon in the European Atlantic Coastal Area and in the West Mediterranean Sea (Gulf of Lions), *Marine Chemistry*, 70, 339–357, [https://doi.org/10.1016/S0304-4203\(00\)00036-0](https://doi.org/10.1016/S0304-4203(00)00036-0), 2000.
- Ferrari, G. M., Bo, F. G., and Babin, M.: Geo-Chemical and Optical Characterizations of Suspended Matter in European Coastal Waters, *Estuarine, Coastal and Shelf Science*, 57, 17–24, [https://doi.org/10.1016/S0272-7714\(02\)00314-1](https://doi.org/10.1016/S0272-7714(02)00314-1), 2003.
- GEBCO Bathymetric Compilation Group 2020: The GEBCO\_2020 Grid - a Continuous Terrain Model of the Global Oceans and Land., <https://doi.org/10.5285/A29C5465-B138-234D-E053-6C86ABC040B9>, 2020.



- Gordon, H. R. and Morel, A. Y.: Remote Assessment of Ocean Color for Interpretation of Satellite Visible Imagery: A Review, Springer US, New York, NY, 1983.
- 345 Guthrie, W. F.: NIST/SEMATECH e-Handbook of Statistical Methods (NIST Handbook 151), <https://doi.org/10.18434/M32189>, 2012.
- Hedges, J., Keil, R., and Benner, R.: What Happens to Terrestrial Organic Matter in the Ocean?, *Organic Geochemistry*, 27, 195–212, [https://doi.org/10.1016/S0146-6380\(97\)00066-1](https://doi.org/10.1016/S0146-6380(97)00066-1), 1997.
- Jerlov, N.: *Optical Oceanography*, Elsevier Publishing Company, New York, 1968.
- Lee, Z., Carder, K. L., Mobley, C. D., Steward, R. G., and Patch, J. S.: Hyperspectral Remote Sensing for Shallow Waters I A Semianalytical  
350 Model, *Applied Optics*, 37, 6329, <https://doi.org/10.1364/AO.37.006329>, 1998.
- Massicotte, P.: PMassicotte/Coastlooc\_data\_paper: V1.0.0, Zenodo, <https://doi.org/10.5281/ZENODO.7708653>, 2023.
- Massicotte, P., Asmala, E., Stedmon, C., and Markager, S.: Global Distribution of Dissolved Organic Matter along the Aquatic Continuum: Across Rivers, Lakes and Oceans, *Science of The Total Environment*, 609, 180–191, <https://doi.org/10.1016/j.scitotenv.2017.07.076>, 2017.
- Massicotte, P., Babin, M., Fell, F., Fournier-Sicre, V., and Doxaran, D.: The COASTLOOC Project Dataset, <https://doi.org/10.17882/93570>,  
355 2023.
- Morel, A. and Bélanger, S.: Improved Detection of Turbid Waters from Ocean Color Sensors Information, *Remote Sensing of Environment*, 102, 237–249, <https://doi.org/10.1016/j.rse.2006.01.022>, 2006.
- Morel, A. and Prieur, L.: Analysis of Variations in Ocean Color: Ocean Color Analysis, *Limnology and Oceanography*, 22, 709–722, <https://doi.org/10.4319/lo.1977.22.4.0709>, 1977.
- 360 O'Reilly, J. E. and Werdell, P. J.: Chlorophyll Algorithms for Ocean Color Sensors - OC4, OC5 & OC6, *Remote Sensing of Environment*, 229, 32–47, <https://doi.org/10.1016/j.rse.2019.04.021>, 2019.
- R Core Team: R: A Language and Environment for Statistical Computing, R Foundation for Statistical Computing, Vienna, Austria, 2022.
- Stramski, D., Reynolds, R. A., Babin, M., Kaczmarek, S., Lewis, M. R., Röttgers, R., Sciandra, A., Stramska, M., Twardowski, M. S., Franz, B. A., and Claustre, H.: Relationships between the Surface Concentration of Particulate Organic Carbon and Optical Properties in the  
365 Eastern South Pacific and Eastern Atlantic Oceans, *Biogeosciences*, 5, 171–201, <https://doi.org/10.5194/bg-5-171-2008>, 2008.
- Sugihara, S., Kishino, M., and Okami, N.: Contribution of Raman Scattering to Upward Irradiance in the Sea, *Journal of the Oceanographical Society of Japan*, 40, 397–404, <https://doi.org/10.1007/BF02303065>, 1984.
- Tassan, S. and Ferrari, G. M.: An Alternative Approach to Absorption Measurements of Aquatic Particles Retained on Filters, *Limnology and Oceanography*, 40, 1358–1368, <https://doi.org/10.4319/lo.1995.40.8.1358>, 1995.
- 370 Tassan, S. and Ferrari, G. M.: Measurement of Light Absorption by Aquatic Particles Retained on Filters: Determination of the Optical Pathlength Amplification by the ‘Transmittance-Reflectance’ Method, *Journal of Plankton Research*, 20, 1699–1709, <https://doi.org/10.1093/plankt/20.9.1699>, 1998.
- Tassan, S. and Ferrari, G. M.: Variability of Light Absorption by Aquatic Particles in the Near-Infrared Spectral Region, *Applied Optics*, 42, 4802, <https://doi.org/10.1364/AO.42.004802>, 2003.
- 375 Van Der Linde, D.: Protocol for Determination of Total Suspended Matter in Oceans and Coastal Zones, Tech. Rep. I.98, 1998.
- Vargas, M., Brown, C. W., and Sapiano, M. R. P.: Phenology of Marine Phytoplankton from Satellite Ocean Color Measurements, *Geophysical Research Letters*, 36, L01 608, <https://doi.org/10.1029/2008GL036006>, 2009.
- Vidussi, F., Claustre, H., Bustillos-Guzmán, J., Cailliau, C., and Marty, J.-C.: Determination of Chlorophylls and Carotenoids of Marine Phytoplankton: Separation of Chlorophyll *a* from Divinylchlorophyll *a* and Zeaxanthin from Lutein, *Journal of Plankton Research*, 18,  
380 2377–2382, <https://doi.org/10.1093/plankt/18.12.2377>, 1996.